

## Correlating Near-Infrared Spectra to Bulk Properties in Polyolefins

Bradley P. Sutliff,<sup>§</sup> Shailja Goyal,<sup>§</sup> Tyler B. Martin,<sup>\*</sup> Peter A. Beaucage, Debra J. Audus, and Sara V. Orski<sup>\*</sup>Cite This: *Macromolecules* 2024, 57, 2329–2338

Read Online

ACCESS |



Metrics &amp; More

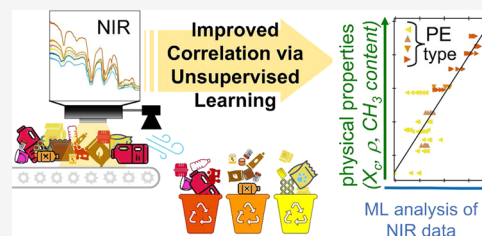


Article Recommendations



Supporting Information

**ABSTRACT:** The industry standard for sorting plastic wastes is near-infrared (NIR) spectroscopy, which offers rapid and nondestructive identification of various plastics. However, NIR does not provide insights into the chain composition, conformation, and topology of polyolefins. Molar mass, branching distribution, thermal properties, and comonomer content are important variables that affect final recyclate properties and compatibility with virgin resins. Heterogeneous mixtures arise through sorting errors, multicomponent materials, or limits on differentiation of polyolefin subclasses leading to poor thermal and mechanical properties. Classic polymer measurement methods can quantify physical properties, which would enable better sorting; however, they are generally too slow for application in commercial recycling facilities. Herein, we leverage the limited chemistry of polyolefins and correlate the structural information from slower measurement methods to NIR spectra through machine learning models. We discuss the success of NIR-property correlations to delineate between polyolefins based on topology.



## INTRODUCTION

Polyolefins (PO) are a vital, structurally complex family of commodity plastics that have both a high global demand and a high potential for recyclability due to their chemical stability and ability to be reprocessed.<sup>1–4</sup> Despite this fact, the recycling rates of postconsumer and postindustrial materials, as well as the utilization rates of recycled PO resins remain low compared to other recycled products like aluminum cans and glass bottles.<sup>2,5,6</sup> As of 2022, approximately 42% of U.S. polymer consumption is POs, yet less than 10% of those materials are recycled effectively.<sup>2</sup> If consumer waste could be properly recycled and reclaimed into a circular economy, there is an estimated economic benefit of as much as 1 trillion USD per year.<sup>7</sup> Unfortunately, there are significant scientific, practical, and societal barriers to PO recycling. One such barrier is the limitation of current sorting technologies at materials recovery facilities (MRFs) and secondary recyclers (SRs). Typically, recycled plastics are sorted at MRFs following the ASTM International Resin Identification Coding System (RIS), specifically D7611M-21,<sup>8</sup> using a variety of manual and automatic sortation schemes. SRs then purchase these materials by the bale to reprocess and sell as postconsumer resin (PCR). While ASTM D7611M-21 classifies resins with some granularity according to the chemical composition and material density, it cannot address the myriad of architectural variations present in POs. PO variations are extensive and enable many unique product designs including rigid containers, blown films, layered packaging, impact-resistant materials, and many others.<sup>2,9</sup> This useful variability, however, complicates the production

of reliable PCR, necessitating careful sorting by either MRFs or SRs.

Despite being chemically “similar”, sorting polyethylenes (PE) and polypropylenes (PP) at recovery facilities is important as these materials are largely incompatible and cannot be easily mixed.<sup>10,11</sup> When they are mixed, they result in significantly degraded properties.<sup>1,11,12</sup> Surprisingly, even many of the subclasses of PE can be incompatible with each other, depending on their topological variation, composition of the blend, and molar mass. For example, the variation between high-density polyethylene (HDPE) and low-density polyethylene (LDPE) can prevent the two materials from fully mixing, resulting in significant defects or compromised mechanical properties for recycled parts.<sup>13</sup>

Furthermore, challenges in PO circularity overlap with classic polymer measurement challenges because the multitude of PO products is made possible through control of interdependent structure–property relationships (e.g., chemical composition, chain topology, crystallization). The breadth of material properties resulting from large varieties and distributions of chain topologies are not well described using broad terms for POs such as PP, HDPE, LDPE, and linear low-density polyethylene (LLDPE) as demonstrated by the range of values present in Table 1. These subclasses differ in

Received: November 8, 2023

Revised: January 11, 2024

Accepted: January 17, 2024

Published: February 28, 2024

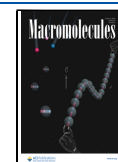


**Table 1. Polyolefin Variability from Literature Examples**

class	subclass	(SCB <sup>a</sup> or CH <sub>3</sub> )/ 1000 C	LCB <sup>a</sup> / 1000 C	refs
PE	HDPE	0–15	0	20, 21, 23–26, this work
PE	LDPE	13–34	2–15	13–18, 23, 25–27
PE	LLDPE	≤40	0	21, 25, 26, 28–30
PP		310–333	0–2	16, 22, 31
PP	PP-co-PE	283–316	0–3	16, 22

<sup>a</sup>denotes short chain branching (SCB) and long chain branching (LCB), respectively.

branching concentration and length which arise from various polymerization mechanisms, comonomers, catalysts, reactor and process conditions that favor different isomers during synthesis.<sup>13–18</sup> Generally, the distinction between high-, low-, and linear low-density PE is specified by their density, as outlined in ASTM D883–22,<sup>19</sup> and are graded as such for appropriate processing and mechanical properties.<sup>17</sup> HDPE polymers have long ethylene backbone chains with minimal branching defects.<sup>20,21</sup> LDPE branching content consists of both short-chain branches (SCB) and long-chain branches (LCB), and the long-chain branches themselves can have differing topologies depending on the polymerization method used.<sup>15,16</sup> SCB are often generally defined as side chains ≤6 carbons off the main chain, and are often reported as methyls per 1000 carbons (CH<sub>3</sub>/1000 C).<sup>15,18,20,22</sup> LCB are generally defined as side chains that are greater than their entanglement molecular weight.<sup>17</sup> These inter- and intrachain defects lower the crystallinity and density in PE polymers. LLDPE polymers have higher fractions of SCB and no significant LCB. Despite the branching differences, LLDPE polymers usually have similar or lower density to LDPE. Additionally, mid- or medium-density PE (MDPE) has been used by some vendors to describe PE with densities and branching content somewhere between those of HDPE and LDPE. PP carries a methyl (–CH<sub>3</sub>) pendant group in the repeat unit leading to roughly one methyl pendant per monomer unit, depending on ethylene comonomer content. The degree of ethylene addition to commercial PP is usually between (1 and 7) % by mass.<sup>22</sup> Despite this addition of ethylene, these polymers are still commercially labeled as PP homopolymers.<sup>22</sup> Larger fractions of ethylene comonomer can be included in random copolymers. Higher ethylene content ((5 to 15) % by mass) is present in PE/PP impact copolymers (PP-co-PE), which, as their name implies, have excellent impact strength even at low temperatures.<sup>22</sup>

To adapt to these broad categories, MRFs and SRs rely on multiple sorting techniques, including hand-sorting, density-based sorting, and a combination of both optical and spectroscopic methods.<sup>10,32</sup> Near-infrared spectroscopy (NIR) has become the industrial workhorse technique used in recycling facilities to sort plastics. NIR can be rapidly executed from a distance in reflection geometry and provide enough rich chemical information, based on the vibrational energies of the polymer chains, to separate by resin codes. NIR can identify subtle structural differences between polymers and, most notably, it is possible to separate PE and PP by exploiting signal differences in the NIR.<sup>33–36</sup> Distinguishing PEs is a larger challenge, as a lower concentration of –CH<sub>3</sub> chain ends from the SCB and main chain represents only a small fraction of total chemical functionality and is not readily observed in NIR spectra. In addition, colorants and other

additives provide extra sorting complications as they alter the NIR signal by introducing new chemistries to the materials. Black pigments in particular absorb a large fraction of the incident light, limiting the observable signal.<sup>33,37</sup>

Further efforts to address challenges in plastics sorting have begun through advances in NIR reflection technology, Raman scattering, and hyperspectral imaging (HSI).<sup>36–39</sup> Recently, chemometrics has advanced the separation technology by resin types in the laboratory, differentiating PE, PP, polystyrene (PS), polyvinyl chloride (PVC), polyethylene terephthalate (PET), and others using partial least-squares discriminant analysis of NIR reflectance data.<sup>33</sup> Despite these improvements in supervised pattern recognition to classify the postconsumer plastics, POs' near-identical chemistries limit the success of these techniques. Even hyperspectral imaging, an extremely data-rich technique, struggles to distinguish the subtle shifts between subclasses of PE.<sup>39</sup> The use of multiple spectroscopic methods, such as NIR or Fourier transform infrared (FTIR) and Raman measurements, coupled with multivariate data analysis has been shown to identify key properties such as density and crystallinity in POs.<sup>38,40,41</sup> FTIR/mid-IR (MIR) can use peak ratios to provide a quantitative value for the branching content, which can then be used to infer trends in crystallinity and density.<sup>38,40,42–44</sup> However, in their current states, both Raman and MIR are impractical for independent use in large-scale sorting operations.<sup>45</sup> A combination of NIR and factor analysis has demonstrated some ability to distinguish between various classes of POs, including HDPE and LDPE blends.<sup>41,46,47</sup> Additionally, both Kim et al. and Sato et al. have demonstrated that partial least-squares regression (PLSR) of NIR spectra may be able to predict properties such as densities, crystallinity, and melting points of PEs made by a single manufacturer.<sup>41,47</sup> However, in both papers, the authors appear to use manufacturer-provided properties and assume they remain constant despite thermal processing. Gosselin et al. demonstrated that these are poor assumptions when they characterized their melt-pressed films of LDPE, HDPE, and PP with NIR, HSI, and differential scanning calorimetry (DSC).<sup>48</sup> Gosselin's work more robustly demonstrated that NIR can be correlated to sample crystallinity by mapping crystallinity across a film; however, they only had one polymer architecture per polymer type.<sup>48</sup>

To enable additional advances in spectra-based characterization and sortation, including HSI, it is essential to form a link between the spectra and physical properties.<sup>49</sup> The subtle changes in conformational isomers of POs yield substantial property changes, which can be described and quantified using robust analytical tools and connected to the observed NIR signal. Specifically, density can be measured via the Archimedes principle,<sup>50</sup> crystallinity is commonly measured using X-ray scattering or melt enthalpy from DSC,<sup>43,48,51,52</sup> and an appropriately configured high-temperature size exclusion chromatography (HT-SEC) system can identify branching content and molar mass distribution.<sup>42</sup> While each of these characterization techniques is impractical for characterization at an MRF or even a secondary recycler, they can easily characterize PO samples in a way that can be connected to the NIR measurements for further analysis. By using physical measurements to inform the spectral interpretations, it may be possible to draw much more information from the spectra and identify the physical characteristics of the polymer samples. This would then enable the rapid quantification of polyolefin isomers with property-specific categorizations to maintain the

quality and control of PCR properties. Additionally, the physical measurements can inform researchers using chemometric and machine learning (ML) techniques by opening the “blackbox” and providing insight into the learning algorithms.

In this work, we combine the chemometric and ML techniques of functional principal component analysis (fPCA) with the NIR spectra of a variety of well-characterized POs sourced from polymer standards and commercial sources. Using appropriate scattering corrections and data processing, we demonstrate that NIR can not only distinguish between POs such as PP and PE but also identify and predict various degrees of bulk density, crystallinity, and SCB for PEs sourced from multiple suppliers. To the authors' knowledge, this is the first time unsupervised dimensionality reduction has been used to correlate NIR with properties of multiple polymer samples across multiple suppliers. While this study serves as a proof of principle, expansion of this work with a greater variety of samples would enable more robust sorting of POs without significant additional requirements for current MRFs and SRs, and therefore increase the value of recycled materials to further incentivize a circular economy. This work would be most helpful to SRs where POs have already been roughly sorted and the facilities are looking to maximize the purity of their PCR.

## MATERIALS AND METHODS

**Samples.** Seven POs, representing commercial plastic samples, were used along with 9 PO samples from the Hawaii Pacific University Polymer Kit 1.0.<sup>53</sup> Additionally, National Institute of Standards and Technology (NIST) PE Standard Reference Materials (SRM<sup>®</sup>) 1473, 1474, and 1476 were included. All samples came in the pellet form. In total, this sample set has 5 HDPEs, 1 MDPE, 7 LDPEs, 2 LLDPEs, 2 PPs, and 2 PP-co-PEs. The type of each source is identified based on classification from the commercial material specification sheets. A summary of the samples and their sources is provided in Table 2.<sup>54</sup>

**Table 2. Summary of the Sample Sources Used in This Study**

source	HDPE	MDPE	LDPE	LLDPE	PP	PP-co-PE
commercial polymers	2	0	2	0	1	2
Hawaii Pacific University Polymer Kit 1.0	2	1	3	2	1	0
NIST	1	0	2	0	0	0

**NIR.** NIR measurements were carried on a Nicolet iS50 NIR module, Thermo Fischer Scientific (Waltham, MA), at 4 cm<sup>-1</sup> resolution and an accumulation of 32 scans with an integrating sphere and an indium gallium arsenide (InGaAs) detector.<sup>54</sup> Internal background and dark corrections were applied to the measurements. Pellets were used as received and filled at least halfway in a 20 mL VWR borosilicate glass scintillation vial (approximately (1 to 2) g) as a representative aliquot of the sample resin. Each sample was measured 6 times, where the vial was shaken between scans in an attempt to redistribute the pellets in the vial and account for local composition variations. The vial was then placed flat on the NIR module centered with the beam path. Additionally, changes in sample vials and vial lids were confirmed not to alter the NIR signal significantly.

**HT-SEC.** High-temperature size exclusion chromatography (HT-SEC) was performed using a Polymer Char GPC-IR instrument with an IR4 detector, a Wyatt Technology Dawn Helios II multiangle light scattering detector (18 angles), and a four-capillary differential viscometer, as well as a Tosoh HT-EcoSEC instrument with

differential refractive index (RI) detection.<sup>54</sup> Samples were dissolved at concentrations between 1 and 2 mg/mL for 60 min at 160 °C with gentle agitation. Separations were conducted at 160 °C using 1,2,4-trichlorobenzene as the eluent, with 300 mg/kg Irganox 1010 added as an antioxidant to the solvent reservoir. 5 μL of dodecane was added to each vial as a flow rate marker. The stationary phase for both systems was a set of 3 Tosoh HT columns (2 Tosoh TSK gel GMH<sub>HR</sub>-H(20) HT2, 13 μm mixed bed, 7.8 mm ID × 30 cm columns, and 1 Tosoh TSK gel GMH<sub>HR</sub>-H(20) HT2, 20 μm, 7.8 mm ID × 30 cm column with an exclusion limit ≈ 4 × 10<sup>8</sup> g/mol). For the Tosoh instrument, narrow dispersity PE standards were used for calibration. For the Polymer Char instrument, narrow dispersity polystyrene standards were used for column calibration. NIST SRM<sup>®</sup> 1475A (linear, broad, HDPE) was used as a linear standard for the viscometer and multiangle light scattering (MALS) detector and to calibrate the voltage response of each. NIST SRM<sup>®</sup> 1478 was used to calibrate the interdetector delay and normalize the photodiode response of the MALS detector. Composition standards consisting of 6, α-olefin copolymer LLDPE standards (poly(ethylene-*stat*-1-octene)), (2.6 to 45.3) CH<sub>3</sub>/1000 C) from Polymer Char were used to calibrate the IR response from the methyl and alkyl absorption bands. A second calibration curve to calibrate the IR was constructed out of blends of PE and PP, where the total areas of the IR responses were plotted against the average SCB content, which was confirmed offline by Nuclear Magnetic Resonance via the manufacturer. While LDPE identification was based on assignment from the manufacturer and long-chain branch content and frequency were not further interrogated in this work, overall LCB content was measured for all polymers, and LDPE LCB content was nominally less than 2 LCB/1000 total carbons for all LDPE samples. Calibration and data analyses were performed with proprietary software from each instrument vendor. Data processing for the HT-SEC data was conducted using a linear Berry formalism to fit the light scattering data for molar mass determinations, and the  $dn/dc$  for all HT-SEC data was fixed at -0.107 mL/g. All injections were done twice, and the reported error on all measurements is one standard deviation of the mean.

**Differential Scanning Calorimetry (DSC).** Crystallinity measurements were carried out on a TA Instruments 2500 differential scanning calorimeter with a heating rate of 10 °C/min in hermetic aluminum pans under a 50 mL/min nitrogen flow. Percent crystallinity was evaluated using the enthalpy of melting  $\Delta H_m$  from the first heating cycle and using the heat of fusion ( $\Delta H_m^0$ ) of 293.6 J/g for PE and 207.1 J/g for PP samples.<sup>55</sup> The crystallinity,  $X_c$ , was calculated via  $X_c = \Delta H_m / \Delta H_m^0$ .

**Density.** While general density ranges for POs are provided in Table 3, actual density measurements were taken for pellet samples

**Table 3. Classification of High-Density (HDPE), Medium-Density (MDPE), Low-Density (LDPE), Linear Low-Density Polyethylenes (LLDPE), and Polypropylene (PP) with Approximate Bulk Density Ranges**

polyolefin classification	density (g·cm <sup>-3</sup> )
HDPE	0.941–0.967 <sup>4</sup>
MDPE <sup>a</sup>	0.926–0.940 <sup>19,52</sup>
LDPE <sup>a</sup>	0.910–0.940 <sup>4</sup>
LLDPE	0.910–0.925 <sup>4,19</sup>
PP	0.902 <sup>19</sup>

<sup>a</sup>Usually produced commercially by free radical polymerization.

using a Mettler Toledo density kit for MS-104S balance, based on ASTM Standard D792–20.<sup>56</sup> Polymer pellet samples were weighed in air and 2-propanol to determine density. Measurements were carried out twice using different pellets, and the mean density and standard error of the mean are reported for each sample.

**Data Analysis and Machine Learning Models.** Data analysis was performed using Python (3.10.8), and example code can be found

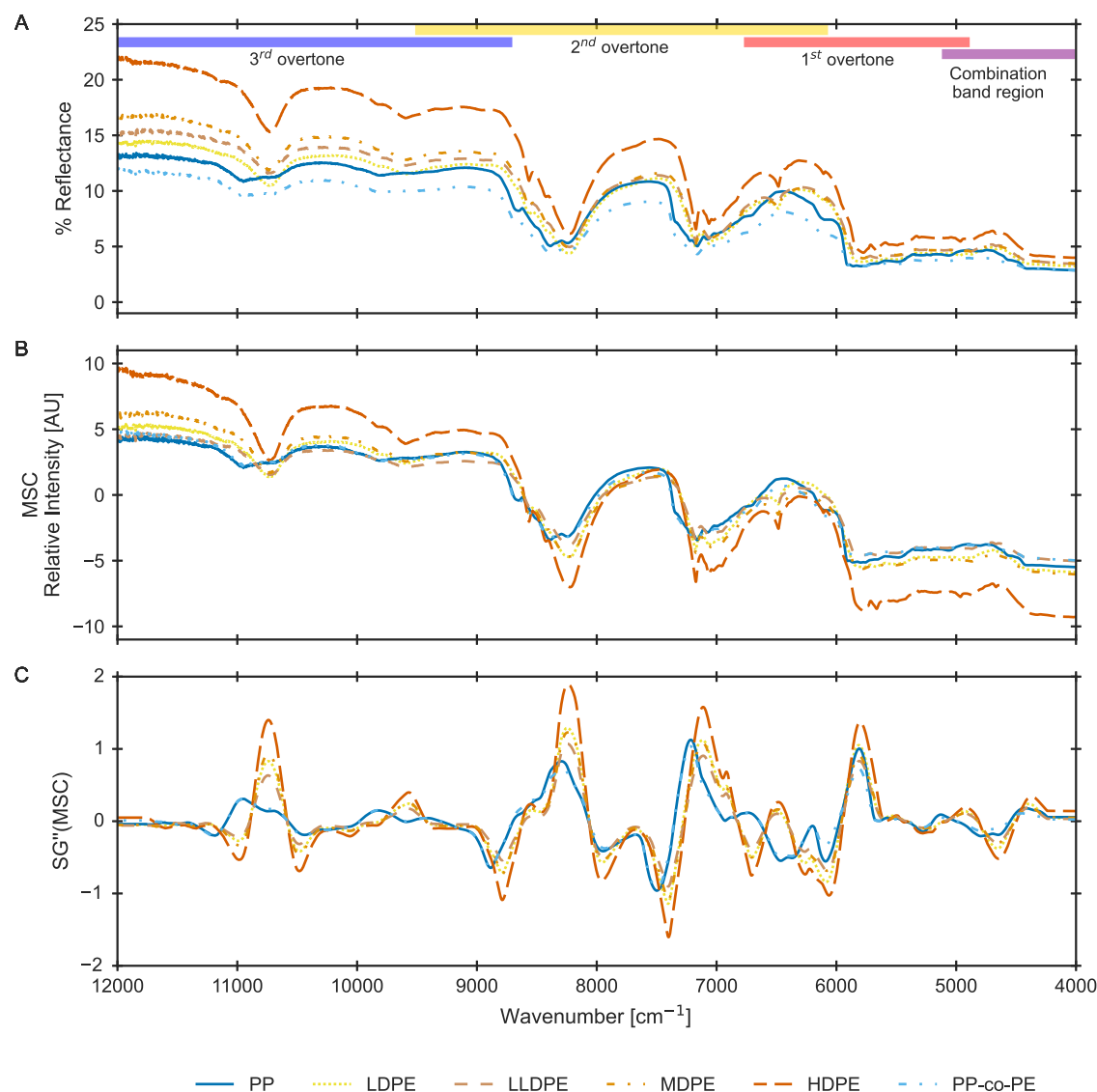


**Figure 1.** Representative NIR spectra and the effects of preprocessing on the data. (A) Raw data, (B) mean scattering correction (MSC), and (C) Savitzky–Golay second derivative and smoothing.

on GitHub repository (usnistgov/nir\_corr\_po).<sup>57</sup> Prior to the application of any ML technique, the NIR data was organized such that each wavenumber represented a single factor or column and each sample replicate represented a row. As discussed in the **Near Infrared Spectroscopy** Section, different preprocessing methods are considered. After preprocessing, the intensities for each wavenumber were standardized (Scikit-learn, 0.24.2) to reflect the variation between samples rather than their absolute values. The scaled data was then reduced by functional principal component analysis (scikit-fda, 0.7.1), using the default parameters. Linear regression quantified the correlation and goodness of fit between the first 4 functional principal components (fPCs) and the density, crystallinity, and SCB. Sliced inverse regression (sliced 0.7.0) modeled density, crystallinity, and SCB content as a linear function of the first 3 fPCs ( $\geq 98\%$  variance). This enables prediction of the polymer characteristics using NIR if new data is preprocessed through the same analysis pipeline.

## RESULTS AND DISCUSSION

**Near Infrared Spectroscopy.** NIR measurements of various PO samples constructed a database of 114 NIR measurements across 19 PO samples. Representative NIR spectra for various subclasses of PE (HDPE, MDPE, LDPE,

LLDPE) and PP (PP, PP-co-PE) are shown in **Figure 1A** in the (4000 to 12,000)  $\text{cm}^{-1}$  range. The NIR spectra for PE classes have tremendous resemblance owing to nearly identical chemistry and only topological differences. However, **Figure 1A** shows that PP spectra are clearly distinguishable even prior to any application of a statistical method (see ranges (11,000 to 10,000)  $\text{cm}^{-1}$  and (7000 to 6000)  $\text{cm}^{-1}$ ). Despite this, further differences between the PE subclasses remain difficult to reliably identify. Some of this difficulty stems from bulk morphology differences between nearly identical polymers, which contribute to deceptive changes in scattered signal intensities.

NIR measurements are especially susceptible to increased scattering due to the shorter wavelengths used in the measurement. While crystallinity and density affect scattering to some extent, sample geometry (film, pellet, powder) has a much greater effect on the NIR signal.<sup>58</sup> To account for this, initial preprocessing steps must be used to minimize bulk scattering effects while emphasizing chemical differences. The most common method for removing bulk scattering is the multiplicative scattering correction (MSC).<sup>58</sup> Ideally, MSC

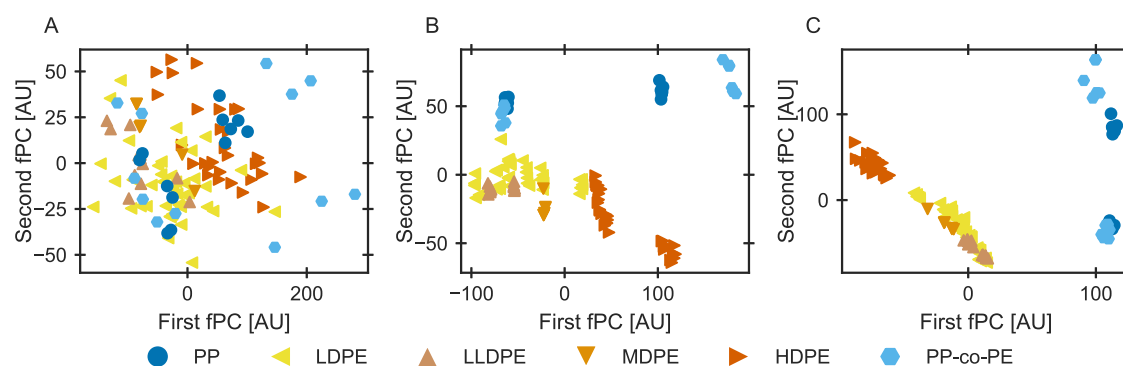


**Figure 2.** fPCA scores plot of (A) raw data, (B) multiplicative scattering corrected (MSC), and (C) Savitzky–Golay second derivative and smoothing after MSC. See the SI for explained variance for each of the first 4 fPCs. All axes are labeled in arbitrary units, [AU].

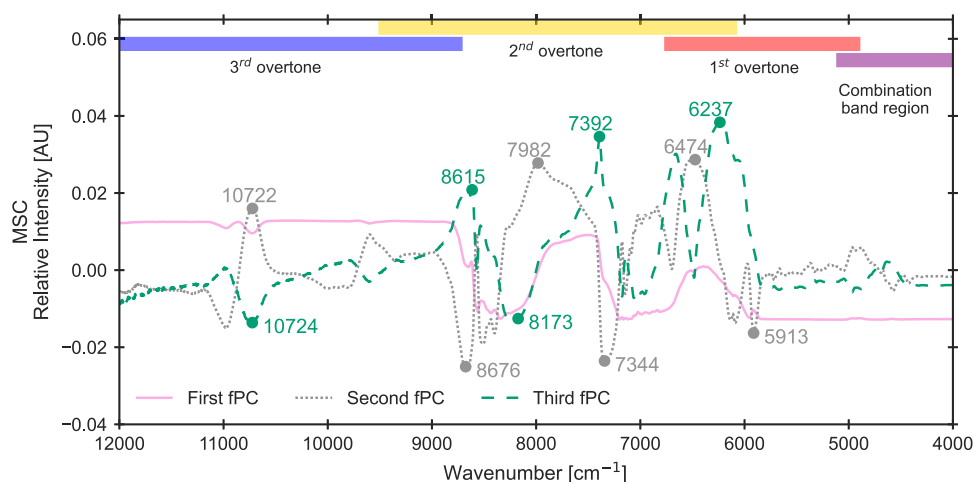


**Figure 3.** fPCA loading plot for the first 3 fPCs of the MSC-corrected data.

compares measured spectra with a scatter-free reference spectrum to remove both multiplicative and additive scattering artifacts. In practice, as in this work, the reference spectrum is often generated as an averaged spectrum based on all similar spectra/samples. Figure 1A,1B demonstrates the effect that this has when applied to all spectra. In this work, each specific polymer sample was measured 6 times (see the Materials and Methods Section), and those 6 replicates were used to generate a reference spectrum for each unique polymer.

Once the bulk scattering is removed, it becomes easier to identify differences in the spectra that may arise from the molecular architectures.<sup>59,60</sup> For instance, in Figure 1B, the intensity at 10722 cm<sup>-1</sup>, the third overtone peak for HDPE samples, is notably more prominent than any other sample. Such differences underscore the potential for NIR to identify differences in polymer subclasses, but the intrinsic density of information and overlapping peaks complicates quantitative analysis for any given range of wavenumbers. Previous research has demonstrated that vibrational spectroscopy can identify changes in these characteristics, just not in the overtone regions of NIR.<sup>42,43</sup> The overtones and combination bands of NIR are directly connected to the mid-IR vibrational spectra, but they are broadened and convoluted, leading mid-IR related peaks to appear as shoulders and slope changes in NIR. This complicates NIR data analysis as it is difficult to distinguish sample changes from noise.

Previous literature has also used Savitzky–Golay smoothing (SG) to differentiate NIR spectra and further highlight spectral

differences based on these peak locations and slope changes.<sup>33,58,61</sup> The second derivative of an SG smoothed (SG<sup>2</sup>) spectrum can be seen in Figure 1C. SG<sup>2</sup> spectra underscore differences between PE and PP, while obscuring differences between the various subclasses of PE. Given that HDPE and LDPE often phase-separate, the preprocessing that enables better PE distinction is preferred, leading analysis away from the SG<sup>2</sup> method, in this context.

**Chemometrics and Functional Principal Component Analysis.** The full effect of these preprocessing steps becomes apparent once the data are analyzed with an ML technique such as principal component analysis (PCA) or functional PCA (fPCA). PCA is a widely used chemometric dimensionality reduction method used on NIR data.<sup>62,63</sup> This technique uses the variance between data points to build a set of linear basis vectors or principal components (PCs) that redescribe the data based on variation between measurements.<sup>62</sup> These components can then be ordered by the percent of variance in the data set that they describe, with the first few PCs capturing most of this variance. Each spectrum containing thousands of points is then reduced to a single number or “score” for each PC, enabling simpler visualization and analysis of the reduced data. This technique can be especially useful for overcoming issues where multiple features or wavelengths follow the same trends, leading to multicollinearity issues when trying to fit regression models.<sup>64–67</sup> An extension of PCA is functional PCA (fPCA) which models the sample data as a linear combination of continuous functions (loadings) instead of

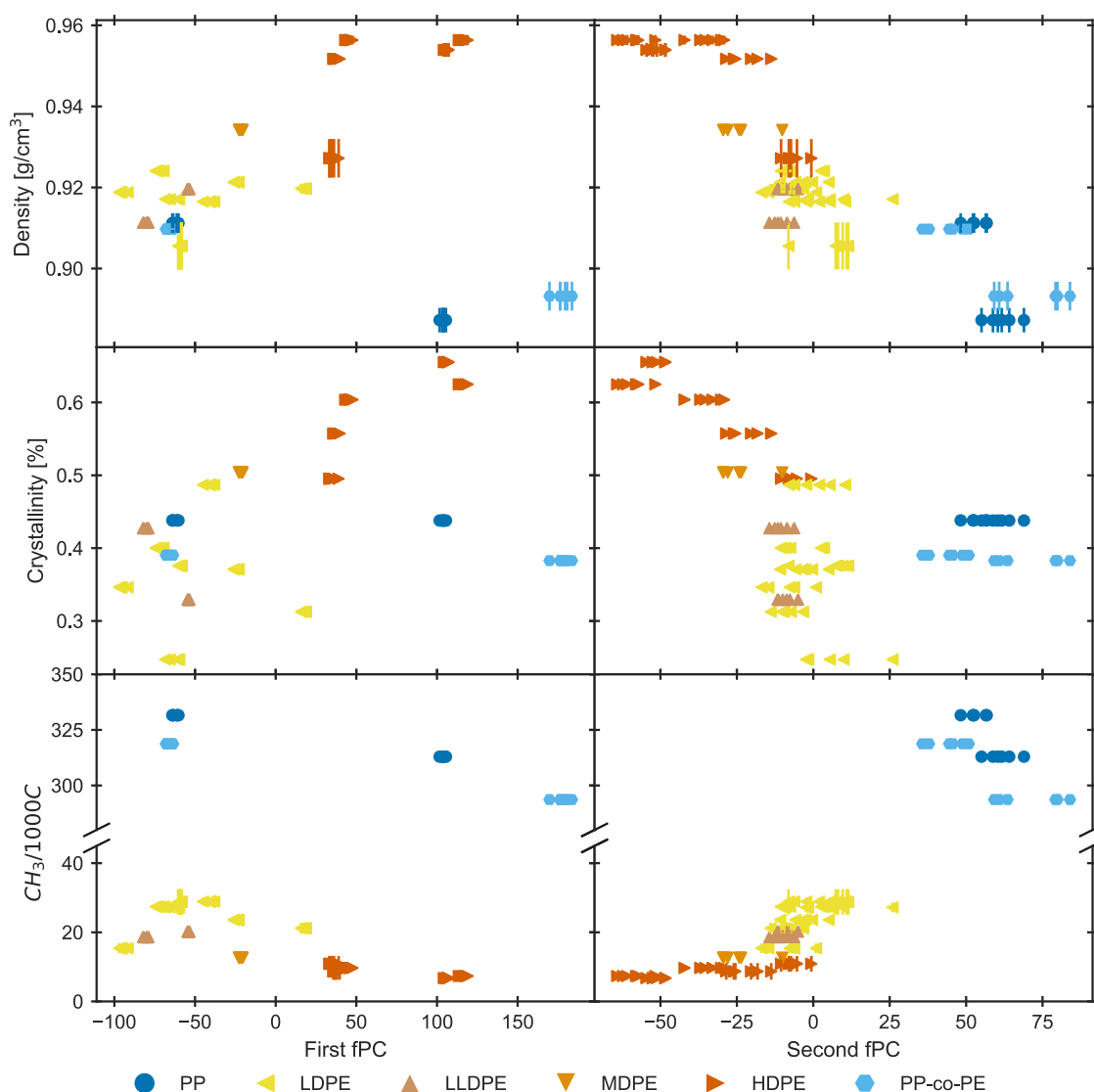


**Figure 4.** Density, crystallinity, and SCB plotted as functions of the first two functional principal components. Density and SCB plots include error bars for the standard error of the mean (SEM) of multiple measurements. Note that the vertical axis for SCB is broken since there is a large gap between the PE and PP branch content.

discrete points stored as vectors.<sup>68</sup> This slight difference allows for statistical analysis with interpolation capabilities, which overcome challenges in comparing spectra of differing resolution.<sup>68</sup> While irrelevant for this data set, as all spectra are taken at the same resolution, we utilized fPCA to allow for comparison with NIR data from future collections on other instruments with different experimental capabilities such as resolution.

Figure 2 displays the reduced data from fPCA, with each spectrum being represented by its first and second fPC scores. It should be noted that Figure 2 is useful for qualitative comparisons, not necessarily quantitative, since fPCA is based on variance between samples, and the differing preprocessing steps will emphasize or limit certain sources of variance.

The raw data have too much variation from scattering artifacts, and chemical sample variation is not well represented in these initial fPCs. Removal of this scattering with MSC enables fPC to distinguish samples (Figure 2B), with the second fPC representing much of the variation between PP and PE. The SG" data (Figure 2C) demonstrates that further

preprocessing can enhance PP and PE distinction. However, it further obfuscates the distinction between the PE subclasses. Overall, we obtained the best separation in various PE classes for MSC preprocessed data without any additional smoothing or derivative processing. With this in mind, further analysis is conducted using only the MSC preprocessed data and the corresponding fPCA-reduced data.

Loading plots from the fPCA enable us to visualize the basis functions or loadings behind the fPC scores and to understand how variation in the MSC-corrected spectra is represented by these loadings. Figure 3 shows the loading plot for the first three fPCs, and the explained variance for each fPC can be found in Table S1. The loading for the first fPC contains mostly broad peaks. These features may arise from minor differences in scattering, such as from microstructural differences in these semicrystalline materials. In contrast, the second and third fPCs have sharp peak-like features in wavenumber regions associated with known overtone bands identified in the literature, e.g., at labeled points between (8700 to 6000)  $\text{cm}^{-1}$ .<sup>69,70</sup> It is important to remember that the peaks in these

loadings do not necessarily correspond with the peaks in the raw NIR spectrum but with the variance between the materials at those points. Therefore, it is as likely that these fPCs identify meaningful changes in the broadening or narrowing of shoulders as it is that they identify meaningful changes in peak heights or locations. With that in mind, many of the peaks depicted in the second and third overtones occur within the overtone regions that would indicate differences in the C–H vibrations.<sup>69</sup> Given that increased levels of crystallization would lead to a restriction in the motions for the C–H vibrations, it is reasonable to think that these signal changes may be correlated with changes in crystallinity or density. These two properties are also closely linked to the SCB content.<sup>42</sup>

To further investigate these correlations, Figure 4 displays the relationships among density, crystallinity, SCB, and the first two fPCs (relationships with the third and fourth fPCs are provided in Figure S1 of the SI). Both components show clear correlation for PE and PP. Table 4 provides the Pearson's

**Table 4. Pearson's Correlation ( $r_{\text{corr}}$ ) and Goodness of Fit ( $r^2$ ), for Density, Crystallinity, and SCB with Respect to the First 2 fPCs**

fPC	property	PE		PP	
		$r_{\text{corr}}$	$r^2$	$r_{\text{corr}}$	$r^2$
1	density	0.85	0.72	−0.90	0.80
1	% crystallinity	0.78	0.61	−0.80	0.06
1	SCB	−0.74	0.55	−0.89	0.80
2	density	−0.86	0.73	−0.66	0.44
2	% crystallinity	−0.80	0.61	−0.09	0.01
2	SCB	0.80	0.64	−0.65	0.42

correlation coefficients ( $r_{\text{corr}}$ ) and the linear goodness of fit ( $r^2$ ) for relationships between the first 2 fPCs and the properties that were measured separately. Both PE and PP display strong correlations ( $|r_{\text{corr}}| \geq 0.5$ ) for almost all combinations of fPCs and properties. While this provides strong evidence of connections between our fPCs and our properties, the  $r^2$  values indicate that a more complex relationship may be appropriate.

#### Regression Models for Prediction of Properties.

Although all of the measured properties are highly correlated with the NIR-derived fPCs, the correlations are not unique to

one property and one fPC as shown in Figure 4 and Table 4. To disentangle this, we applied sliced inverse regression (SIR) to the properties and fPCs for the subclasses of PE. PP was removed due to the limited number of PP samples in our data set. Similar to fPCA, SIR is a linear dimensionality reduction technique. The key difference is that unlike fPCA, SIR is a supervised ML technique, meaning that it requires both the inputs, fPC values in this case, and the output, a property in this case. Here, the dimension of SIR is limited to one, such that each property can be described by a single variable ( $X\hat{\beta}_{\text{SIR}}$ ) where  $X$  is a vector of the scores from the first 3 fPCs and  $\hat{\beta}_{\text{SIR}}$  is a vector of the 3 corresponding linear coefficients. Only 3 fPCs were chosen as they account for over 95% of the total variance in the sample set. The values of  $X\hat{\beta}_{\text{SIR}}$  vary for each property and are provided in Table S2. The results are shown in Figure 5, and Pearson's correlation scores are in Table 5. A

**Table 5. Pearson's Correlation Scores for the Measured Properties of PE with One Another and with  $X\hat{\beta}_{\text{SIR}}$**

	density	crystallinity	SCB	$X\hat{\beta}_{\text{SIR}}$
density	1	0.84	−0.83	0.89
crystallinity		1	−0.75	0.87
SCB			1	−0.88

linear regression model was then fit to describe each property as a function of  $X\hat{\beta}_{\text{SIR}}$ . All three models had  $r^2 \geq 0.75$  and  $r_{\text{corr}} \geq 0.85$ , providing strong evidence of their ability to predict these properties to a useful degree using only NIR inputs. However, it is essential to note that while a linear relationship is assumed to compute these quantities, the actual relationship may be nonlinear.

As previously mentioned, the values of  $X\hat{\beta}_{\text{SIR}}$  depend on the property (see Table 5). Since the fPCs are correlated with one another, the values of  $X\hat{\beta}_{\text{SIR}}$  cannot be used to determine the relative contributions of each fPC to the physical quantities of interest. Thus, we utilized the feature importance ranking measure (FIRM) analysis.<sup>71,72</sup> FIRM quantifies the relative contributions of each fPC to the final prediction of each property while also taking the correlations of the fPCs with one another into account. The results, shown in Table 6, clarify that no individual fPC yields a majority contribution to the prediction of the density, crystallinity, or SCB. Instead, the first and second fPCs contribute similar amounts of information

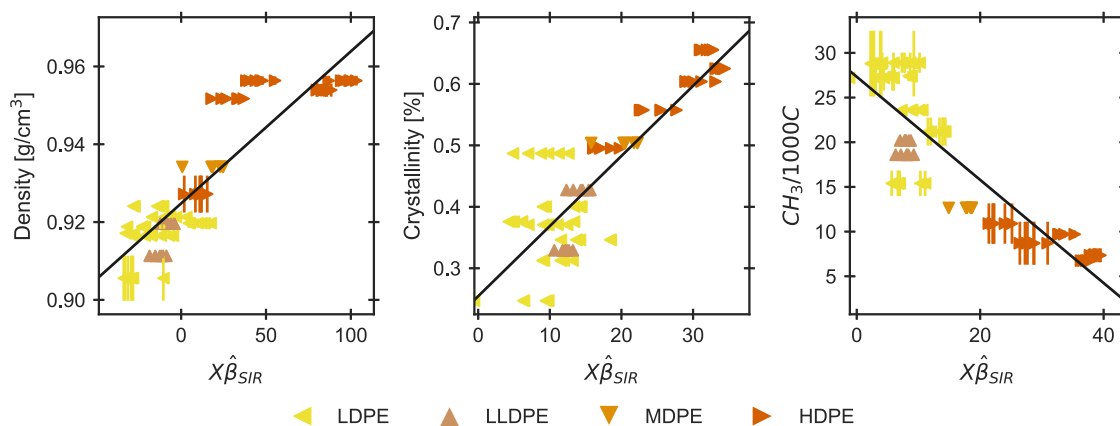


**Figure 5.** Scatter plots of the density, crystallinity, and SCB after slice inversion regression with 3 fPCs to allow the prediction of properties by assigning weight coefficients to each fPC score.  $r^2$  values for the linear regression models are 0.79, 0.75, and 0.77, respectively.

**Table 6. Relative Contribution of Each fPC in the Prediction of the Given Physical Quantity, as Determined by FIRM**

fPC	density	crystallinity	SCB
first	0.406	0.369	0.459
second	0.423	0.439	0.446
third	0.171	0.192	0.095

( $\approx 40\%$  to  $45\%$  each) while the third fPC contributes the remaining predictive information ( $\approx 10\%$  to  $20\%$ ). The minimal contribution from the third fPC is expected since, from fPCA, it explains less than  $10\%$  of the variance in the NIR data.

To further understand the relative contributions of the fPCs, we look at Figures 2B and 3. Figure 2B shows that the second fPC predominantly separates PP from PE, while the first enables distinctions between the PE subclasses. These differences may bias the FIRM analysis, given that the fPCA was performed using the PP data, but the SIR and FIRM analyses excluded the PP due to lack of samples. With this in mind, Figure 3 shows that the second fPC has its most prominent peaks at ( $10722$ ,  $7982$ , and  $6474$ )  $\text{cm}^{-1}$ . The first and last of these correspond directly to PE and PP differences visible in Figure 1A,B, but the  $7982$   $\text{cm}^{-1}$  value is much less clear. Meanwhile, the first fPC has its most notable peaks around ( $7500$  and  $6400$ )  $\text{cm}^{-1}$ , which correspond to peaks in the PE, but even manual qualitative analysis of these spectral differences would be difficult with the MSC-corrected data.

Finally, while the data set size used to develop these models was ultimately small in the context of ML, it demonstrates tremendous potential for amplifying the information taken from NIR data if polymer scientists curate their data effectively. As our model greatly expands upon previous work<sup>46–48</sup> to create a more generalizable model for PEs, additional well-characterized samples should help further refine models and provide predictive power for polymers besides PE, or for predicting additional properties such as additive concentration. To this point, it should be emphasized that when building or expanding such a data set, the quality of the data set may provide more power than quantity. This work focused largely on density and crystallinity and thus required a data set spanning those properties. In expanding this model, it would be most beneficial to add samples such as ultrahigh molecular weight polyethylene to expand the range of prediction. In any case, this work enables sorting of the most common PEs at a rapid rate, using currently implemented technologies, and could help SRs produce higher-quality recyclates in the near future. Additionally, these techniques could be used by resin manufacturers to monitor the quality of their products in a rapid, nondestructive manner.

## CONCLUSIONS

Using a data set containing samples from various classes of POs (5 HDPEs, 1 MDPE, 7 LDPEs, 2 LLDPEs, 2 PPs, and 2 PP-co-PEs), this work expanded upon the correlations between NIR data and properties such as density, crystallinity, and SCB. We studied the effect of various preprocessing methods on NIR data and the resultant effects on the outcomes of an unsupervised ML model through fPCA. Deconstruction of the fPC loadings revealed direct connections to expected overtone bands in the raw NIR spectra. Additionally, the fPCs and corresponding scores obtained from this analysis revealed

direct correlations between the scores and the measured properties of the polymers. Using a supervised data reduction model (SIR), linear regression, and the PE data, we were able to predict these properties using only NIR spectra and careful data analysis techniques. This data pipeline would enable MRFs and SRs to characterize POs much more accurately while using their current methodologies. Further study using correlative, unsupervised models also has the potential to improve the measurement of PO feedstocks, particularly as more sustainable polymers, additives, and higher percentages of PCR are incorporated and are continuously expanding the complexity of commercial polymers.

## ASSOCIATED CONTENT

### Supporting Information

The Supporting Information is available free of charge at <https://pubs.acs.org/doi/10.1021/acs.macromol.3c02290>.

Additional experimental results including explained variance ratios; SIR coefficients; and correlations with fPC 3 and 4 (PDF)

## AUTHOR INFORMATION

### Corresponding Authors

**Tyler B. Martin** – Materials Science and Engineering Division, National Institute of Standards and Technology, Gaithersburg, Maryland 20899, United States; [orcid.org/0000-0001-7253-6507](https://orcid.org/0000-0001-7253-6507); Email: [tyler.martin@nist.gov](mailto:tyler.martin@nist.gov)

**Sara V. Orski** – Materials Science and Engineering Division, National Institute of Standards and Technology, Gaithersburg, Maryland 20899, United States; [orcid.org/0000-0002-3455-0866](https://orcid.org/0000-0002-3455-0866); Email: [sara.orski@nist.gov](mailto:sara.orski@nist.gov)

### Authors

**Bradley P. Sutliff** – Materials Science and Engineering Division, National Institute of Standards and Technology, Gaithersburg, Maryland 20899, United States; [orcid.org/0000-0002-2399-3071](https://orcid.org/0000-0002-2399-3071)

**Shailja Goyal** – Materials Science and Engineering Division, National Institute of Standards and Technology, Gaithersburg, Maryland 20899, United States

**Peter A. Beaucauge** – NIST Center for Neutron Research, National Institute of Standards and Technology, Gaithersburg, Maryland 20899, United States

**Debra J. Audus** – Materials Science and Engineering Division, National Institute of Standards and Technology, Gaithersburg, Maryland 20899, United States; [orcid.org/0000-0002-5937-7721](https://orcid.org/0000-0002-5937-7721)

Complete contact information is available at: <https://pubs.acs.org/10.1021/acs.macromol.3c02290>

### Author Contributions

<sup>§</sup>B.P.S. and S.G. contributed equally to this work.

### Notes

The authors declare no competing financial interest.

## ACKNOWLEDGMENTS

This work was primarily supported by the NIST circular economy initiative along with NIST Information Technology Laboratory. The authors thank Dr. Kathryn Beers for her insight and support and Dr. Robert Ivancic for his recommendations regarding FIRM analysis.

## REFERENCES

- (1) Yin, S.; Tuladhar, R.; Shi, F.; Shanks, R. A.; Combe, M.; Collister, T. Mechanical reprocessing of polyolefin waste: A review. *Polym. Eng. Sci.* **2015**, *55*, 2899–2909.
- (2) Westlie, A. H.; Chen, E. Y.-X.; Holland, C. M.; Stahl, S. S.; Doyle, M.; Trenor, S. R.; Knauer, K. M. Polyolefin Innovations toward Circularity and Sustainable Alternatives. *Macromol. Rapid Commun.* **2022**, *43*, No. e2200492.
- (3) Serranti, S.; Gargiulo, A.; Bonifazi, G. Classification of polyolefins from building and construction waste using NIR hyperspectral imaging system. *Resour., Conserv. Recycl.* **2012**, *61*, 52–58.
- (4) Kupolati, W. K.; Sadiku, E. R.; Ibrahim, I. D.; Adeboje, A. O.; Kambole, C.; Ojo, O. O. S.; Eze, A. A.; Paige-Green, P.; Ndambuki, J. M. The Use of Polyolefins in Geotextiles and Engineering Applications. In *Polyolefin Fibres*, 2nd ed.; Ugbole, S. C. O., Ed.; Woodhead Publishing, 2017; pp 497–516.
- (5) Bowyer, J.; Bratkovich, S.; Fernholz, K.; Frank, M.; Groot, H.; Howe, J.; Pepke, E. *Understanding Steel Recovery and Recycling Rates and Limitations to Recycling*; Dovetail Partners, Inc.: 2015; 1–12.
- (6) Dijkgraaf, E.; Gradus, R. Are Bottle Banks Sufficiently Effective for Increasing Glass Recycling Rates? *Sustainability* **2021**, *13*, No. 9540.
- (7) Korhonen, J.; Honkasalo, A.; Seppälä, J. Circular Economy: The Concept and its Limitations. *Ecol. Econ.* **2018**, *143*, 37–46.
- (8) ASTM International. *Standard Practice for Coding Plastic Manufactured Articles for Resin Identification*; ASTM D7611M-21: West Conshohocken, PA, 2022.
- (9) Schyns, Z. O. G.; Shaver, M. P. Mechanical Recycling of Packaging Plastics: A Review. *Macromol. Rapid Commun.* **2021**, *42*, No. e2000415.
- (10) Ip, K.; Testa, M.; Raymond, A.; Graves, S. C.; Gutowski, T. Performance evaluation of material separation in a material recovery facility using a network flow model. *Resour., Conserv. Recycl.* **2018**, *131*, 192–205.
- (11) Vogt, B. D.; Stokes, K. K.; Kumar, S. K. Why is Recycling of Postconsumer Plastics so Challenging? *ACS Appl. Polym. Mater.* **2021**, *3*, 4325–4346.
- (12) Van Belle, A.; Demets, R.; Mys, N.; Van Kets, K.; Dewulf, J.; Van Geem, K.; De Meester, S.; Ragaert, K. Microstructural Contributions of Different Polyolefins to the Deformation Mechanisms of Their Binary Blends. *Polymers* **2020**, *12*, No. 1171.
- (13) Hameed, T.; Hussein, I. A. Effect of short chain branching of LDPE on its miscibility with linear HDPE. *Macromol. Mater. Eng.* **2004**, *289*, 198–203.
- (14) Kulin, L. I.; Meijerink, N. J.; Starck, P. Long and short chain branching frequency in low density polyethylene (LDPE). *Pure Appl. Chem.* **1988**, *60*, 1403–1415.
- (15) Liu, P.; Liu, W.; Wang, W.-J.; Li, B.-G.; Zhu, S. A comprehensive review on controlled synthesis of long-chain branched polyolefins: Part 1, single catalyst systems. *Macromol. React. Eng.* **2016**, *10*, 156–179.
- (16) Liu, W.; Liu, P.; Wang, W.-J.; Li, B.-G.; Zhu, S. A comprehensive review on controlled synthesis of long-chain branched polyolefins: Part 2, multiple catalyst systems and prepolymer modification. *Macromol. React. Eng.* **2016**, *10*, 180–200.
- (17) Liu, P.; Liu, W.; Wang, W.-J.; Li, B.-G.; Zhu, S. A comprehensive review on controlled synthesis of long-chain branched polyolefins: Part 3, characterization of long-chain branched polymers. *Macromol. React. Eng.* **2017**, *11*, No. 1600012.
- (18) Sauter, D. W.; Taoufik, M.; Boisson, C. Polyolefins, a Success Story. *Polymers* **2017**, *9*, No. 185.
- (19) ASTM International. *Standard Terminology Relating to Plastics*, ASTM D883-23: West Conshohocken, PA, 2023.
- (20) Aggarwal, S. L.; Sweeting, O. J. Polyethylene: Preparation, Structure, And Properties. *Chem. Rev.* **1957**, *57*, 665–742.
- (21) Peacock, A. *Handbook of Polyethylene: Structures: Properties, and Applications*; CRC Press, 2000.
- (22) Malpass, D. B.; Band, E. *Introduction to Industrial Polypropylene: Properties, Catalysts Processes*; John Wiley & Sons, 2012.
- (23) Agamalian, M.; Alamo, R. G.; Kim, M. H.; Londono, J. D.; Mandelkern, L.; Wignall, G. D. Phase Behavior of Blends of Linear and Branched Polyethylenes on Micron Length Scales via Ultra-Small-Angle Neutron Scattering. *Macromolecules* **1999**, *32*, 3093–3096.
- (24) Londono, J. D.; Narten, A. H.; Wignall, G. D.; Honnell, K. G.; Hsieh, E. T.; Johnson, T. W.; Bates, F. S. Composition Dependence of the Interaction Parameter in Isotopic Polymer Blends. *Macromolecules* **1994**, *27*, 2864–2871.
- (25) Lee, H. S.; Denn, M. M. Blends of linear and branched polyethylenes. *Polym. Eng. Sci.* **2000**, *40*, 1132–1142.
- (26) Cho, K.; Lee, B. H.; Hwang, K.-M.; Lee, H.; Choe, S. Rheological and mechanical properties in polyethylene blends. *Polym. Eng. Sci.* **1998**, *38*, 1969–1975.
- (27) Hill, M. J.; Puig, C. C. Liquid-liquid phase separation in blends of a linear low-density polyethylene with a low-density polyethylene. *J. Appl. Polym. Sci.* **1997**, *65*, 1921–1931.
- (28) Gabriel, C.; Lilge, D. Comparison of different methods for the investigation of the short-chain branching distribution of LLDPE. *Polymer* **2001**, *42*, 297–303.
- (29) Hili, M.; Barham, P. J. Interpretation of phase behaviour of blends containing linear low-density polyethylenes using a ternary phase diagram. *Polymer* **1994**, *35*, 1802–1808.
- (30) Musikabhumma, K.; Spaniol, T. P.; Okuda, J. Synthesis of branched polyethylenes by the tandem catalysis of silica-supported linked cyclopentadienyl-amido titanium catalysts and a homogeneous dibromo nickel catalyst having a pyridylimine ligand. *J. Polym. Sci., A: Polym. Chem.* **2003**, *41*, 528–544.
- (31) Gloger, D.; Mileva, D.; Albrecht, A.; Hubner, G.; Androsch, R.; Gahleitner, M. Long-Chain Branched Polypropylene: Effects of Chain Architecture, Melt Structure, Shear Modification, and Solution Treatment on Melt Relaxation Dynamics. *Macromolecules* **2022**, *55*, 2588–2608.
- (32) Dubanowitz, A. J. Design of a Materials Recovery Facility (Mrf) for Processing the Recyclable Materials of New York City's Municipal Solid Waste. M.Sc. Thesis. School of Engineering and Applied Science, Columbia University. 2000.
- (33) Rani, M.; Marchesi, C.; Federici, S.; Rovelli, G.; Alessandri, I.; Vassalini, I.; Ducoli, S.; Borgese, L.; Zacco, A.; Bilo, F.; Bontempi, E.; Depero, L. E. Miniaturized Near-Infrared (MicroNIR) Spectrometer in Plastic Waste Sorting. *Materials* **2019**, *12*, No. 2740.
- (34) Sem, V. Interpretability of selected variables and performance comparison of variable selection methods in a polyethylene and polypropylene NIR classification task. *Spectrochim. Acta, Part A* **2021**, *258*, No. 119850.
- (35) Serranti, S.; Luciani, V.; Bonifazi, G.; Hu, B.; Rem, P. C. An innovative recycling process to obtain pure polyethylene and polypropylene from household waste. *Waste Manage.* **2015**, *35*, 12–20.
- (36) Serranti, S.; Palmieri, R.; Bonifazi, G.; Cózar, A. Characterization of microplastic litter from oceans by an innovative approach based on hyperspectral imaging. *Waste Manage.* **2018**, *76*, 117–125.
- (37) Rozenstein, O.; Puckrin, E.; Adamowski, J. Development of a new approach based on midwave infrared spectroscopy for post-consumer black plastic waste sorting in the recycling industry. *Waste Manage.* **2017**, *68*, 38–44.
- (38) Bredács, M.; Barretta, C.; Castillon, L. F.; Frank, A.; Oreski, G.; Pinter, G.; Gergely, S. Prediction of polyethylene density from FTIR and Raman spectroscopy using multivariate data analysis. *Polym. Test.* **2021**, *104*, No. 107406.
- (39) Vidal, C.; Pasquini, C. A comprehensive and fast microplastics identification based on near-infrared hyperspectral imaging (HSI-NIR) and chemometrics. *Environ. Pollut.* **2021**, *285*, No. 117251.
- (40) Hagemann, H.; Snyder, R. G.; Peacock, A. J.; Mandelkern, L. Quantitative infrared methods for the measurement of crystallinity and its temperature dependence: polyethylene. *Macromolecules* **1989**, *22*, 3600–3606.

- (41) Kim, M.; Noh, J.; Chung, H. Comparison of near-infrared and Raman spectroscopy for the determination of the density of polyethylene pellets. *Anal. Chim. Acta* **2009**, *632*, 122–127.
- (42) Orski, S. V.; Kassekert, L. A.; Farrell, W. S.; Kenlaw, G. A.; Hillmyer, M. A.; Beers, K. L. Design and Characterization of Model Linear Low-Density Polyethylenes (LLDPEs) by Multidetector Size Exclusion Chromatography. *Macromolecules* **2020**, *53*, 2344–2353.
- (43) Mallapragada, S. K.; Narasimhan, B. *Encyclopedia of Analytical Chemistry*; John Wiley & Sons, Ltd: Chichester, UK, 2006.
- (44) Kavesh, S.; Schultz, J. M. Meaning and measurement of crystallinity in polymers: A Review. *Polym. Eng. Sci.* **1969**, *9*, 331–338.
- (45) Olscher, C.; Jandric, A.; Zafiu, C.; Part, F. Evaluation of Marker Materials and Spectroscopic Methods for Tracer-Based Sorting of Plastic Wastes. *Polymers* **2022**, *14*, No. 3074, DOI: 10.3390/polym14153074.
- (46) Miller, C. E. Use of near-infrared spectroscopy to determine the composition of high-density/low-density polyethylene blend films. *Appl. Spectrosc.* **1993**, *47*, 222–228.
- (47) Sato, H.; Shimoyama, M.; Kamiya, T.; Amari, T.; Šašić, S.; Ninomiya, T.; Siesler, H. W.; Ozaki, Y. Near Infrared Spectra of Pellets and Thin Films of High-Density, Low-Density and Linear Low-Density Polyethylenes and Prediction of Their Physical Properties by Multivariate Data Analysis. *J. Near Infrared Spectrosc.* **2003**, *11*, 309–321.
- (48) Gosselin, R.; Rodrigue, D.; Duchesne, C. On-line prediction of crystallinity spatial distribution across polymer films using NIR spectral imaging and chemometrics methods. *Can. J. Chem. Eng.* **2008**, *86*, 869–878.
- (49) DesLauriers, P. J.; Rohlfing, D. C. Estimating slow crack growth performance of polyethylene resins from primary structures such as molecular weight and short chain branching. *Macromol. Symp.* **2009**, *282*, 136–149.
- (50) International Organization for Standardization. *Plastics – Methods for Determining the Density of Non-Cellular Plastics – Part 1: Immersion Method, Liquid Pycnometer Method and Titration Method*. ISO 1183-1:2019; Geneva, Switzerland, 2019.
- (51) Snyder, C. R.; Nieuwendaal, R. C.; DeLongchamp, D. M.; Luscombe, C. K.; Sista, P.; Boyd, S. D. Quantifying Crystallinity in High Molar Mass Poly(3-hexylthiophene). *Macromolecules* **2014**, *47*, 3942–3950.
- (52) Abareshi, M.; Zebarjad, S. M.; Goharshadi, E. K. Crystallinity Behavior of MDPE-Clay Nanocomposites Fabricated using Ball Milling Method. *J. Compos. Mater.* **2009**, *43*, 2821–2830.
- (53) Hawai'i Pacific University Center for Marine Debris Research Polymers Kit 1.0. <https://www.hpu.edu/cnccs/cmdr/products-and-services.html> (accessed: May 30, 2023).
- (54) Any identification of software, equipment, instruments, companies, or materials in this work is done so for the express purposes of completeness and understanding. Such identification does not imply recommendation or endorsement by the National Institute of Standards and Technology, nor does it imply that the materials or equipment identified are necessarily the best available for the purpose.
- (55) Blaine, R. L. *Thermal Applications Note: Polymer Heats of Fusion*, TA Instruments, 2003.
- (56) ASTM International. *Standard Test Methods for Density and Specific Gravity (Relative Density) of Plastics by Displacement; D792-20*: West Conshohocken, PA, 2020.
- (57) SutSutliff, B. P.; Goyal, S.; Martin, T. B.; Beaucage, P. A.; Audus, D. J.; Orski, S. V. Correlating Near-Infrared Spectra to Bulk Properties in Polyolefins, 2023. <https://datapub.nist.gov/od/id/mds2-3022>.
- (58) Rinnan, Å.; Van Den Berg, F.; Engelsen, S. B. Review of the most common pre-processing techniques for near-infrared spectra. *Trends Analyt. Chem.* **2009**, *28*, 1201–1222.
- (59) Okada, T.; Mandelkern, L. Effect of morphology and degree of crystallinity on the infrared absorption spectra of linear polyethylene. *J. Polym. Sci., Part A-2* **1967**, *5*, 239–262.
- (60) Mizushima, M.; Kawamura, T.; Takahashi, K.; Nitta, K.-H. In situ near-infrared spectroscopic studies of the structural changes of polyethylene during melting. *Polym. J.* **2012**, *44*, 162–166.
- (61) Savitzky, A.; Golay, M. J. E. Smoothing and differentiation of data by simplified least squares procedures. *Anal. Chem.* **1964**, *36*, 1627–1639.
- (62) Bro, R.; Smilde, A. K. Principal component analysis. *Anal. Methods* **2014**, *6*, 2812–2831.
- (63) Lever, J.; Krzywinski, M.; Altman, N. Principal component analysis. *Nat. Methods* **2017**, *14*, 641–642.
- (64) Perez, L. V. Principal component analysis to address multicollinearity. <https://www.whitman.edu/documents/academics/mathematics/2017/perez.pdf> (accessed: October 2, 2023).
- (65) Lafi, S. Q.; Kaneene, J. B. An explanation of the use of principal-components analysis to detect and correct for multicollinearity. *Prev. Vet. Med.* **1992**, *13*, 261–275.
- (66) Chigozie Kelechi, A. Regression and Principal Component Analyses: A Comparison Using Few Regressors. *Am. J. Math. Stat.* **2012**, *2*, 1–5.
- (67) Maitra, S.; Yan, J. Principle component analysis and partial least squares: Two dimension reduction techniques for regression. *Appl. Multivar. Stat. Models* **2008**, 79–90.
- (68) Shang, H. L. A survey of functional principal component analysis. *ASTA Adv. Stat. Anal.* **2014**, *98*, 121–142.
- (69) Shimoyama, M.; Ninomiya, T.; Sano, K.; Ozaki, Y.; Higashiyama, H.; Watari, M.; Tomo, M. Near infrared spectroscopy and chemometrics analysis of linear low-density polyethylene. *J. Near Infrared Spectrosc.* **1998**, *6*, 317–324.
- (70) Foster, G. N.; Row, S. B.; Griskey, R. G. Infrared spectrometry of polymers in the overtone and combination regions. *J. Appl. Polym. Sci.* **1964**, *8*, 1357–1361.
- (71) Zien, A.; Krämer, N.; Sonnenburg, S.; Rätsch, G. The Feature Importance Ranking Measure. In *Machine Learning and Knowledge Discovery in Databases*; Springer, 2009; Vol. 5782, pp 694–709.
- (72) Zien, A.; Krämer, N.; Sonnenburg, S.; Rätsch, G. In *The Feature Importance Ranking Measure*, Machine Learning and Knowledge Discovery in Databases: European Conference, ECML PKDD 2009, Bled, Slovenia, September 7–11, 2009, Proceedings, Part II 20; Springer, 2009; pp 694–709.